Available online at www.sciencedirect.com
ScienceDirect
International Journal of Thermal Sciences 47 (2008) 1077–1085
International Journal of Thermal Sciences
www.elsevier.com/locate/ijts

An approach to entropy analysis of a latent heat storage module

Aytunc Erek [a,1], Ibrahim Dincer [b,*]

[a] *Department of Mechanical Engineering, Dokuz Eylul University, Izmir, Turkey*
[b] *Faculty of Engineering and Applied Science, University of Ontario Institute of Technology (UOIT), 2000 Simcoe Street North, Oshawa, Ontario L1H 7K4, Canada*

Received 27 May 2007; received in revised form 6 August 2007; accepted 6 August 2007

Available online 6 September 2007

Abstract

This paper deals with an entropy and exergy efficiency analysis of a latent heat storage system (around a cylindrical tube) during charging process. First, a numerical model is developed and solved through the governing equations for the heat transfer fluid (HTF), pipe wall and phase change material for different parameters (shell radius and pipe length, *Re* number, inlet temperature of HTF, etc.). Second, extensive parametric studies are conducted to investigate how the solidification fronts, heat stored, heat transfer rates, entropy generation number and exergy efficiency change with time, particularly dimensionless time (the Fourier number). Third, the model results are compared with some experimental data of one of the authors, and a good agreement is obtained for various parameters. The results show that entropy generation is crucial in such systems and should be minimized in order to increase the exergy efficiency and hence the system performance.

Keywords: Phase change; Solidification; Latent heat storage; Heat transfer; Entropy generation; Exergy efficiency

Introduction

Thermal energy storage (TES) technology has recently received high attention as one of the primary solutions to the electrical power imbalance between production and demand. Especially, increased cooling demand results in higher electricity demand during the peak hours of summer days. To decrease this peak load and to balance electric production and demand, off-peak electricity during night is stored as cold energy storage by producing cold water or ice to be utilizing by the cooling system in the day time. Some other advantages of TES are the ability to use energy more efficiently and to avoid increasing the capacity for higher demand.

Out of all the various heat storage developments in the area, the latent heat storage is still the most favorable storage medium due to its large capacity to store heat. A number of studies have been conducted to analyze the thermal behavior of latent heat storage systems. Some detailed reviews and technical details about latent energy storage system have been provided elsewhere [1–4].

Many suggest that shell-and-tube type heat exchanger is the most promising device as a latent heat storage system that requires high efficiency for a minimum volume. Studies related to shell-and-tube type of exchanger configuration have been carried out by various researchers (e.g., [5–10]). In such an energy storing unit, the phase change material (PCM) fills the gap between the shell and the tubes in which heat transfer fluid (HTF) flows, also serves to convey the stored energy to and from the unit. A theoretical model of the shell-and-tube type unit for storing energy has been reported by Ismail and Alves [5]. Cao and Faghri [6,7] have also modeled a similar problem at which both the heat charging and the recovery processes have been performed by the circulating fluid. For both models, the shell wall of the unit was assumed to be adiabatic. Using the enthalpy model, the problem of storing

* Corresponding author.
E-mail address: ibrahim.dincer@uoit.ca (I. Dincer).
[1] Currently on his sabbatical leave at University of Ontario Institute of Technology.

1290-0729/$ – see front matter
doi:10.1016/j.ijthermalsci.2007.08.002

Nomenclature

c, c_p	specific heat	$\mathrm{J\,kg^{-1}\,K^{-1}}$
C^0	heat capacity, $c * \rho$	$\mathrm{J\,m^{-3}\,K^{-1}}$
C	$C^0/(c_l \,.\, \rho_l)$	
C_{sl}	$(c_s \,.\, \rho_s)/(c_l \,.\, \rho_l)$	
D	inside diameter of the circular pipe	m
Ex	Exergy	J
Fo	Fourier number, $\alpha_f \,.\, t/D^2$	
H	enthalpy	$\mathrm{J\,kg^{-1}}$
HTF	heat transfer fluid	
k	thermal conductivity	$\mathrm{W\,m^{-1}\,K^{-1}}$
K	dimensionless thermal conductivity (k/k_l)	
K_{sl}	k_s/k_l	
L	length of pipe	m
$\dot{m}$	mass flow rate	$\mathrm{kg\,s^{-1}}$
N_s	entropy generation number	
Nu	Nusselt number	
PCM	phase change material	
Pe_f	fluid Peclet number, $Re_f \,.\, Pr_f$	
Pr_f	fluid Prandtl number, ν_f/α_f	
q^0	heat transfer rate	W
q	dimensionless heat transfer rate per volume, $\frac{q^0}{V^0_{\mathrm{TES}}} \frac{D^2}{\alpha_L . \Delta H}$	
Q^0	total stored energy	J
Q	dimensionless total stored energy per volume, $Q^0/(\Delta H \,.\, V^0_{\mathrm{TES}})$	
r	radial coordinate	m
R	dimensionless radial direction, r/D or solidification front	
Re_f	fluid Reynolds number, $4\dot{m}/\pi D\mu$	
s	specific entropy	$\mathrm{J\,kg^{-1}\,K^{-1}}$
S^0	source term	$\mathrm{J\,m^{-3}}$
S	dimensionless source term, $S^0/\rho_l \,.\, c_l(T_m - T_{\mathrm{in}})$	
	entropy	$\mathrm{J\,K^{-1}}$
Ste	Stefan number	
t	time	s
T	temperature	K or °C
TES	thermal energy storage	
U	overall heat transfer coefficient	$\mathrm{W\,m^{-2}\,K^{-1}}$
x	axial coordinate	m
X	dimensionless axial direction, x/D	

Greek symbols

α	thermal diffusivity	$\mathrm{m^2\,s^{-1}}$
θ	dimensionless temperature, $(T - T_m)/(T_m - T_{\mathrm{in}})$	
$\delta\theta_m$	$\delta T_m/(T_m - T_{\mathrm{in}})$	
ΔH	latent heat of PCM	$\mathrm{J\,m^{-3}}$
μ	dynamic viscosity	$\mathrm{N\,s\,m^{-2}}$
ρ	density	$\mathrm{kg\,m^{-3}}$
ν	kinematic viscosity	$\mathrm{m^2\,s^{-1}}$
ψ	second law (exergy) efficiency	

Subscripts

f	transfer fluid
i	initial condition, or inner radius of pipe
inf	outside of the thermal storage tank
in	inlet
l	liquid PCM
m	mushy phase
o	outer radius of pipe or environmental
out	outlet
s	solid PCM
w	container wall or surface

energy in a shell-and-tube type unit was also solved by Bellecci and Conti [9]. Cao and Faghri [6] have studied the latent heat storage systems for both annular and countercurrent flows and numerically determined that the storage system with the countercurrent flow was an efficient way to absorb heat energy. Lee and Jones [11] developed a stand-along analytical model for an ice-on-coil thermal energy storage system with both charging and discharging modes, and validated the numerical results with the experimental ones. Erek et al. [12,13] and Ermis et al. [14] studied effect of flow parameters on energy stored for different configurations. Trp [15,16] developed a complete model using enthalpy formulation for external melt on tube.

In this study the authors have extended their earlier works [12–14] by investigating various heat transfer and thermodynamic parameters (e.g., solidification fronts, heat transfer rate, entropy generation number, exergy efficiency) during the charging process of the shell-and-tube latent heat storage and how such parameters change with time. The model results are also compared with the experimental data for model verification purposes.

Modeling

Heat transfer analysis

A schematic representation of the physical model for a shell-and-tube energy storage unit is shown in Fig. 1. The PCM fills the annular space, around the tube of inner radius r_o and outer radius r_{inf}, while heat transfer fluid flows inside the tube. The tube wall has inside and outside radius of r_i and r_o, respectively. This study is different from our previous ones (e.g., [12–14]) as heat gain from the environment is taken into account. In the present numerical model, the heat gain changes in proportion to temperature difference between PCM temperature near wall and environment temperature. In other words,

$$q''_{\mathrm{gain}} = U \,.\, (T_0 - T_{\mathrm{PCM}}) \tag{1}$$

where U is overall heat transfer coefficient and the calculated U value from the experimental setup is used in the numerical model as well. The thermophysical properties of the PCM, tube wall and heat transfer fluid are independent of temperature, but the properties of the PCM are different in the solid and liquid

Table 1
Thermophysical properties of HTF, tube wall and PCM

Material	Temperature or phase	ρ (kg m^{-3})	c_p (J kg^{-1} K^{-1})	k (W m^{-1} K^{-1})	α (m^2 s^{-1})	μ (Pa s)	ΔH (J m^{-3})
HTF	−10 °C	838.594	2252.917		1.053E−07	0.0030	–
	−15 °C	842.940	2208.537	0.199	1.069E−07	0.0034	–
	−20 °C	847.286	2148.665		1.093E−07	0.0038	–
Tube wall		8800	420	52	1.407E−05	–	–
PCM (water, $T_m = 0$ °C)	Liquid	999.8	4217	0.561	1.33E−07	–	333.5E06
	Solid	916.8	2040	2.2	–	–	

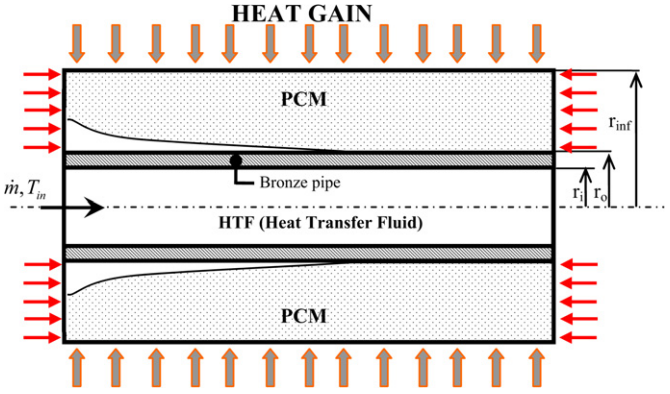

Fig. 1. A schematic view of shell-and-tube type latent heat storage module.

phases. Thermophysical properties of HTF, tube and PCM are given in Table 1. Initially, the system is set to a temperature of T_i higher than T_m. Suddenly, HTF having temperature T_{in} lower than T_m flows in the tube and solidification occurs around the tube. In formulating a mathematical model to represent this physical system, the system is divided into following three subsections; (i) tube flow of heat transfer fluid, (ii) the tube wall, (iii) the region filled by the phase change material.

In the analysis, the following dimensionless variables and groups are employed:

$$R = \frac{r}{D}, \quad X = \frac{x}{D}, \quad Fo = \frac{\alpha_f \,.\, t}{D^2}$$
$$\theta = \frac{T - T_m}{T_m - T_{\text{in}}}, \quad \delta\theta_m = \frac{\delta T_m}{(T_m - T_{\text{in}})}$$
$$Re_f = \frac{4m}{\pi D \mu_f}, \quad Pr_f = \frac{\gamma_f}{\alpha_f}, \quad Pe_f = Re_f \,.\, Pr_f$$
$$Ste = \frac{c_l \,.\, \rho_l (T_m - T_{\text{in}})}{\Delta H}, \quad C = \frac{C^0}{\rho_l c_l}, \quad K = \frac{k}{k_l}$$

Assuming that axial conduction is negligible and fully developed conditions exist at the tube inlet, the dimensionless energy equation of the heat transfer fluid can be expressed as

$$\frac{\partial \theta_b}{\partial Fo} = 4Nu(\theta_w - \theta_b) - Re_f Pr_f \frac{\partial \theta}{\partial X} \tag{2}$$

The quasi-steady assumption is applied to convective heat transfer inside the tube. Transient convection is considered inside the tube as a series of steady state forced convection problems. For laminar flow, the local Nusselt number can be obtained by an analytical method with arbitrary varying temperature at the tube wall which is described by (e.g., [17,18]).

$$(Nu_b)_j = \frac{\sum_{k=1}^{j} \Delta\theta_k \sum_{n=0}^{\infty} G_n \exp[-\frac{2\lambda_n^2}{Pe}(X - (k-1)\Delta X)]}{2\sum_{k=1}^{j} \Delta\theta_k \sum_{n=0}^{\infty} \frac{G_n}{\lambda_n^2} \exp[-\frac{2\lambda_n^2}{Pe}(X - (k-1)\Delta X)]} \tag{3}$$

where $\Delta\theta_k = (\theta_{Ri})_k - (\theta_{Ri})_{k-1}$ and $j = \text{int}(\frac{X}{\Delta X}) + 1$. The values of constant G_n and eigenvalues λ_n is available elsewhere (e.g., [17]).

For the pipe wall, the energy equation is well known as the two-dimensional heat conduction equation:

$$\frac{\partial \theta}{\partial Fo} = \frac{\alpha_l}{\alpha_f}\left[\frac{1}{R}\frac{\partial}{\partial R}\left(K R \frac{\partial \theta}{\partial R}\right) + \frac{\partial}{\partial X}\left(K \frac{\partial \theta}{\partial X}\right)\right] \tag{4}$$

As the initial temperature of the system is considered to be the same or close to the phase change temperature, the natural convection effect around the tube can be neglected. The heat conduction in the PCM is described by a temperature transforming method using a fixed grid numerical model [6]. This model assumes that solidification process occurs over a range of phase change temperature from $T_m - \delta T_m$ to $T_m + \delta T_m$, but it can also be successfully used to simulate solidification process occurring at a single temperature by taking a small range of phase change temperature, $2\delta T_m$. The dimensionless energy equation for the PCM is written as

$$\frac{\partial (C\theta)}{\partial Fo} = \frac{\alpha_l}{\alpha_f}\left(\frac{1}{R}\frac{\partial}{\partial R}\left(K R \frac{\partial \theta}{\partial R}\right) + \frac{\partial}{\partial X}\left(K \frac{\partial T}{\partial X}\right)\right) - \frac{\partial S}{\partial \tau} \tag{5}$$

where

$$C = C(\theta) = \begin{cases} C_{sl}, & \theta < -\delta\theta_m \quad \text{Solid} \\ \frac{1}{2}(1 + C_{sl}) + \frac{1}{2\,Ste\,\delta\theta_m}, & -\delta\theta_m \leqslant \theta \leqslant \delta\theta_m \quad \text{Mushy} \\ 1, & \theta > \delta\theta_m \quad \text{Liquid} \end{cases} \tag{6}$$

$$S = S(\theta) = \begin{cases} C_{sl}\delta\theta_m, & \theta < -\delta\theta_m \quad \text{Solid} \\ \frac{1}{2}\delta\theta_m(1 + C_{sl}) + \frac{1}{2\,Ste}, & -\delta\theta_m \leqslant \theta \leqslant \delta\theta_m \quad \text{Mushy} \\ C_{sl}\delta\theta_m + \frac{1}{Ste}, & \theta > \delta\theta_m \quad \text{Liquid} \end{cases} \tag{7}$$

$$K = K(\theta) = \begin{cases} K_{sl}, & \theta < -\delta\theta_m \quad \text{Solid} \\ K_{sl} + \frac{(1-K_{sl})(\theta+\delta\theta_m)}{2\delta\theta_m}, & -\delta\theta_m \leqslant \theta \leqslant \delta\theta_m \quad \text{Mushy} \\ 1, & \theta > \delta\theta_m \quad \text{Liquid} \end{cases} \tag{8}$$

The initial and boundary conditions can be written as follows:

- Initial condition ($\tau = 0$):

$$0 \leqslant X \leqslant L/D, \; 0 \leqslant R \leqslant R_{\text{inf}} \quad \rightarrow \theta = \theta_i$$

- Boundary conditions ($\tau > 0$):

$0 \leqslant R < 0.5,\ X = 0: \quad \rightarrow \theta = \theta_{\text{in}} = -1$

$0 \leqslant R < 0.5,\ X = L/D: \quad \rightarrow \dfrac{\partial \theta}{\partial X} = 0$

$0.5 \leqslant R \leqslant R_{\text{inf}},\ X = 0 \text{ and } X = L/D: \quad \rightarrow q'' = q''_{\text{gain}}$

$R = 0.5,\ 0 < X < L/D:$

$$\rightarrow -K_w \left(\frac{\partial \theta}{\partial R}\right)_{R=0.5} = Nu_b \,.\, K_f (\theta_b - \theta_w)$$

$R = R_o,\ 0 < X < L/D:$

$$\rightarrow -K_w \left(\frac{\partial \theta}{\partial R}\right)_{R=R_0^-} = -K \left(\frac{\partial \theta}{\partial R}\right)_{R=R_0^+}$$

$R = R_{\text{inf}},\ 0 < X < L/D: \quad \rightarrow q'' = q''_{\text{gain}}$

The temperature distribution inside the solution domain can be calculated by solving the energy equations defined by Eqs. (2)–(8). The solution procedure used for solving these energy equations is control volume approach described by (e.g., [19]). Assuming the bulk temperature approach in the pipe flow, local Nusselt number is determined by using Eq. (3) for laminar flow or by using empirical correlation for turbulent flow. On the other hand, thermal conductivity, k, is calculated by harmonic mean method at the control surface. Semi implicit solver, [20], is used for solving the discretization equations of energy equations. Using this solver, the CPU time is reduced a great amount for a single iteration and this solver requires the less storage than the other solvers such as Gauss–Seidel iteration method.

Since energy equation for the PCM is a non-linear heat conduction equation, iterations are needed during each time step. For a given time step, convergence is declared at the $(k+1)$th iteration when $|\theta_{i,j}^{k+1} - \theta_{i,j}^{k}| \leqslant 10^{-6}$. The numerical results are then verified by testing the resulting predictions for independence of the grid size, time-step and other parameters. The grid size used for the solution was 200 (axial) × 100 (radial) with a time step $\Delta\tau = 0.001$. In addition, in PCM, non-uniform grid size is used with a successive ratio = 1.04.

Furthermore, the overall energy balance is checked during the calculation process to verify the numerical results. At a time step, the change heat storage in PCM and tube wall must be equal to the total energy supplied by the heat transfer fluid as follows,

$$\int_0^{\tau} \frac{\pi}{4} \,.\, Pe_f \,.\, C_f \,.\, (\theta_{b,\text{out}} + 1) \,.\, \mathrm{d}\tau = \int_0^{L} \int_{R_i}^{R_{\text{inf}}} 2\pi \,.\, R \,.\, (H - H_i) \,.\, \mathrm{d}R \,.\, \mathrm{d}X \tag{9}$$

where $H = C \times T + S$ stands for total enthalpy at the control volume. The left side of Eq. (9) represents the thermal energy supplied by the heat transfer fluid and the right side of equation represents the thermal stored energy in the PCM and pipe wall. In calculation procedure, the numerical deviation between two sides of Eq. (9) is taken less than 2%.

The second law analysis

By neglecting the pressure drop in TES module as shown in Fig. 1, the entropy generation rate ($\dot{S}_{\text{gen}}$) can be expressed as:

$$\dot{S}_{\text{gen}} = \dot{m}(s_{\text{out}} - s_{\text{in}}) - \frac{q^0_{\text{gain}}}{T_o} + \Delta\dot{S}_{\text{HTF}} + \Delta\dot{S}_{\text{wall}} + \Delta\dot{S}_{\text{PCM}} \tag{10}$$

Taking specific volumes in HTF remain nearly constant during the process,

$$\dot{S}_{\text{gen}} = \dot{m} c_{P,\text{HTF}} \ln\left(\frac{T_{\text{out}}}{T_{\text{in}}}\right) - \frac{q^0_{\text{gain}}}{T_o} + \Delta\dot{S}_{\text{HTF}} + \Delta\dot{S}_{\text{wall}} + \Delta\dot{S}_{\text{PCM}} \tag{11}$$

The first term on right-hand side of Eq. (11) is the entropy generation rate due to heat removal of fluid flow in the pipe, the second term is the entropy generation due to heat gain, and the last three terms represent entropy storage rate. The entropy storage rates in HTF, pipe wall and PCM can be written, respectively, as

$$\begin{aligned} \Delta\dot{S}_{\text{HTF}} &= \iiint_{V_{\text{HTF}}} \left(\frac{\mathrm{d}s}{\mathrm{d}t}\right) \,.\, \rho \,.\, \mathrm{d}V \\ \Delta\dot{S}_{\text{wall}} &= \iiint_{V_{\text{wall}}} \left(\frac{\mathrm{d}s}{\mathrm{d}t}\right) \,.\, \rho \,.\, \mathrm{d}V \\ \Delta\dot{S}_{\text{PCM}} &= \iiint_{V_{\text{PCM}}} \left(\frac{\mathrm{d}s}{\mathrm{d}t}\right) \,.\, \rho \,.\, \mathrm{d}V \end{aligned} \tag{12}$$

where $\frac{\mathrm{d}s}{\mathrm{d}t} = \frac{s - s^0}{\Delta t}$ denote specific entropy deviation with time, and s and s^0 denote, respectively, specific entropy at present and previous time increments. The total entropy generation can be determined by using Eq. (11) as follows:

$$S_{\text{gen}} = \int_{t=0}^{t} \left[\dot{m} c_{P,\text{HTF}} \ln\left(\frac{T_{\text{out}}(t)}{T_{\text{in}}}\right) - \frac{q^0_{\text{gain}}(t)}{T_o} + \Delta\dot{S}_{\text{HTF}} + \Delta\dot{S}_{\text{wall}} + \Delta\dot{S}_{\text{PCM}}\right] \mathrm{d}t \tag{13}$$

The entropy generation number, N_s for TES system can be expressed as [21,22]:

$$N_s = \frac{S_{\text{gen}} \,.\, T_o}{Ex_{\text{in}}} \tag{14}$$

where Ex_{in} represents total exergy inlet.

In the TES system, second law or exergy analysis allows to determine the maximum potential associated with the incoming thermal energy. The maximum potential can be retained or recovered if the thermal energy undergoes processes in a reversible manner. Since actual processes are irreversible, losses in the potential of exergy recovery occur in the real system. Thus, exergy analysis both quantitatively and qualitatively specifies TES practical limitations by providing losses in a form that directly measure lost thermal exergy.

For any TES system, an exergy balance for the entire TES processes which involves charging, storing and discharging can be written as follows.

$$\text{Exergy input} - (\text{Exergy recovered} + \text{Exergy loss}) - \text{Exergy destroyed} = \text{Exergy accumulation} \quad (15)$$

Since thermal behavior of TES system for only charging period is studied in this work, Eq. (15) can be shortened as:

$$Ex_{\text{flow}} - Ex_{Q\text{gain}} - Ex_{\text{destruction}} = \Delta Ex_{\text{storage}} \quad (16)$$

dividing Eq. (16) by Ex_{flow},

$$1 - \frac{Ex_{Q\text{gain}}}{Ex_{\text{flow}}} - \frac{Ex_{\text{destruction}}}{Ex_{\text{flow}}} = \frac{\Delta Ex_{\text{storage}}}{Ex_{\text{flow}}} \quad (17)$$

The exergy (second-law) efficiency of TES system is defined by the following equation.

$$\psi = \frac{\Delta Ex_{\text{storage}}}{Ex_{\text{flow}}} \quad (18)$$

where Ex_{flow} is total flow exergy of HTF ($Ex_{\text{in}} - Ex_{\text{out}}$).

In this study, the new modified entropy generation number is used instead of defined in previous studies. The new modified entropy generation number is given as follows:

$$N_s = \frac{S_{\text{gen}} \,.\, T_o}{Ex_{\text{flow}}} \quad (19)$$

Substituting Eqs. (18) and (19) into Eq. (17) gives,

$$\psi = 1 - N_s - \frac{Ex_{Q\text{gain}}}{Ex_{\text{flow}}}$$

Case study

In order to verify the model presented above, we use some experimental data taken from Erek et al. [12]. In that study, experimental unit consists of the flow system, heat transfer test section and temperature measurement system. The heat transfer test section is composed of an energy storage tank having dimensions of 420 mm × 570 mm × 500 mm (as width × length × height), tube and phase change material around this tube. To visualize the photograph the solidification fronts around the tube, a digital camera used and desired data are transmitted to a PC. To reduce the heat transfer through the walls of storage tank, the base of the tank is supported with 50 mm thick Styrofoam layer. The side walls and the top wall are covered with 3 cm thick Styrofoam layer. The tube carrying the HTF was a one-piece unit and was produced by machining a solid bronze (87.2% Cu, 6.57% Sn, 4.13% Zn and 1.97% Pb) cylinder. The tube has length of 480 mm, and the inner and outer tube radius of 10 mm and 15 mm respectively. A reservoir for the heat transfer fluid, a constant temperature circulating bath, a variable speed pump, a flow meter, a hydrodynamic entry section are parts of consisting of the flow system. The hydrodynamic entry section length is chosen long enough (∼ 240 diameter, 6500 mm) to provide fully developed flow conditions for the heat transfer fluid at inlet of the energy storage unit. Ethyl-alcohol (CH_3–CH_2OH) is used as the heat transfer fluid to assure liquid behavior at such a low temperature range.

The temperature measuring system consists of temperature sensing elements (thermocouples) and data logger system. The inlet and outlet temperatures of the heat transfer fluid, the temperatures of the points on the outer pipe wall, the temperatures for detecting the variation in water tank, and ambient and constant temperature bath temperatures were measured with copper–constantan thermocouples. The temperatures were read with a multi-channel digital thermometer. All thermocouples used in experiments are type T of gage no. 24 and are calibrated by a constant temperature bath filled with Ethyl-alcohol.

The pure water used as the PCM preliminarily cooled down to the temperature of 0.3°C is pumped into the insulated storage tank. The total amount of water stored in the tank is 110 liters and at a level such that the finned tube becomes oriented at the horizontal symmetry line of the tank. Three different inlet temperatures of −10, −15 and −20 °C and six different flow rates are studied. The flow rates are chosen so that Re number varies between 500 and 7000. Thus, a total of 15 experimental runs were done. More details of experimental procedure can be found in [12–14].

Results and discussion

Before presenting the numerical results for the thermal storage system, the mathematical model was checked with experimental results. Fig. 2 shows the comparison of the solidification fronts along axial coordinate for different Fourier numbers obtained by numerical method and experimental study. In this comparison, the inlet temperature of the HTF and *Re* number is taken to be −15 °C and 1000, respectively. It can be seen that the agreement between the two results is excellent. The reason of that solidification front in numerical study forms in step difference is numerical model used in study. Another comparison is ones of stored energy for different Reynolds numbers as shown in Fig. 3. Total stored energy is calculated by added stored sensible energy, latent energy and heat gain in the experimental study. Also, it can be seen from this figure that agreement between the numerical results and experimental data is very good.

In this study, a series of 81 parametric experiments was performed to assess the overall thermal behavior of TES unit for the design and operating parameters summarized in Table 2. As

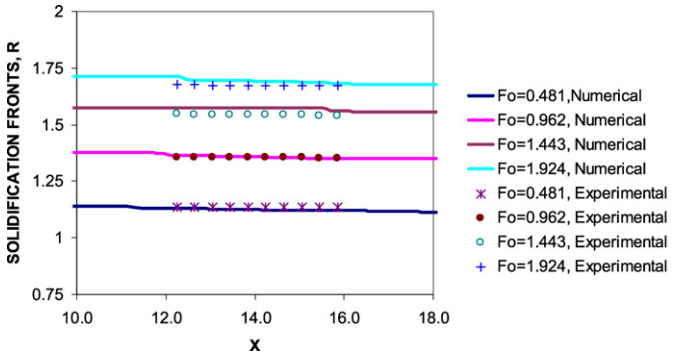

Fig. 2. Comparison of the numerical results of solidification fronts with experimental data.

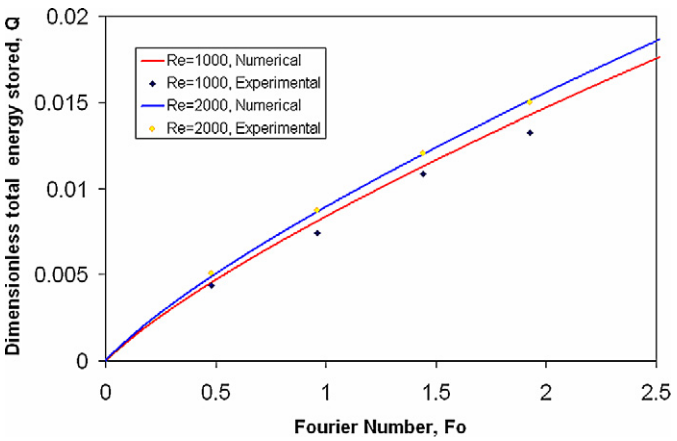

Fig. 3. Comparison of the numerical and experimental results on total energy storage.

Table 2
Design and operating parameters

Design parameters	PCM	Water
	HTF	Ethyl alcohol
	Pipe wall	Bronze
	Inner and outer radius of pipe	0.50 and 0.75
	Shell radius, R_{inf}	2, 3, 5
	Length of pipe, X_L	20, 50, 100
Operating parameters	Reynolds number, Re	500, 1000, 2000
	Inlet temperature of HTF, T_{in}	-10, -15, $-20\,^{\circ}C$
	Initial temperature of TES unit, T_i	$0.3\,^{\circ}C$
	Environmental temperature, T_o	$16.85\,^{\circ}C$ (290 K)

the dimensionless shell radius and length of TES unit are chosen as the important design parameters, on the other hand, the Reynolds number and the inlet temperature of HTF are chosen as the important operating parameters.

In all previous studies, heat gain from environment was not taken into account. Actually, the primary parameter of TES in thermal behavior is the heat gain and the energy and exergy efficiencies of a system depend on the heat gain. In this work, the heat gain has been added to the numerical model and the desired results have been more accurate and realistic than previous ones. Fig. 4 shows the effect of design parameters on heat gain for $Re = 1000$ and $T_{in} = -15\,^{\circ}C$. In order to make better comparison, the heat gain is given in dimensionless form and per TES volume and this structure will use the other presentations. The dimensionless heat gain per total energy storage volume is defined as

$$q = \frac{q^0}{V^0_{TES}} \frac{D^2}{\alpha_L \,.\, \Delta H}$$

As seen from Fig. 4, the heat gain per volume increases as shell radius and length of TES decrease.

Fig. 5 shows the heat transfer rate per volume as a function of time for different design parameters (shell radius and length of TES) and $Re = 1000$ and $T_{in} = -15\,^{\circ}C$. In this study, only charging process is studied and this process may be investigated by dividing into three sub processes. At first time period, thermal energy is stored in the system as sensible and latent. During of this time period, solidification fronts arrive at the outer wall

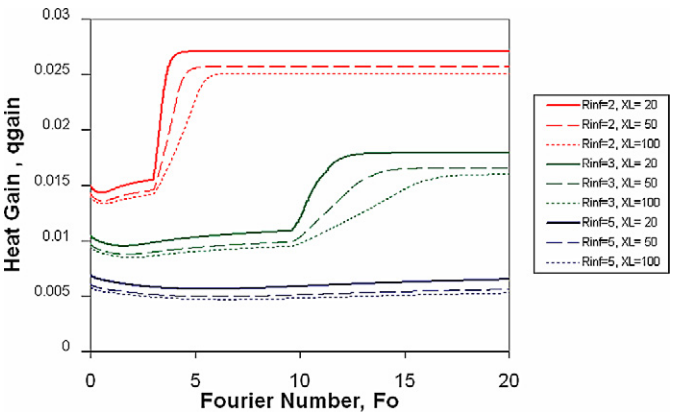

Fig. 4. Effect of design parameters on heat gain for $Re = 1000$ and $T_{in} = -15\,^{\circ}C$.

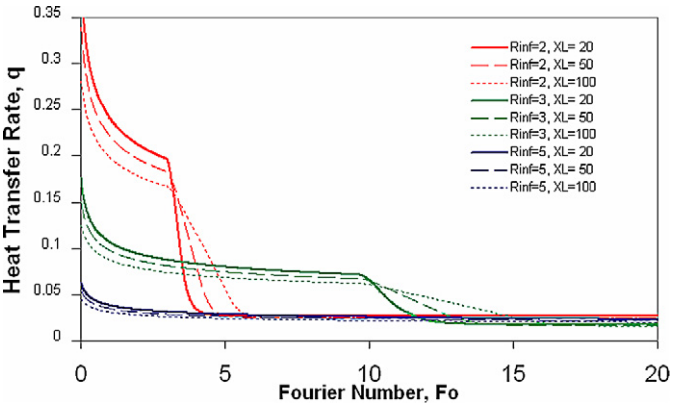

Fig. 5. Effect of design parameters on heat transfer rate for $Re = 1000$ and $T_{in} = -15\,^{\circ}C$.

and solidification finishes. In the second time periods, sensible heat is stored until the PCM temperature decreases to the inlet temperature of HTF. After this time period, the thermal energy storage does not occur and HTF supplies the heat gain. In the light of these definitions, it is clear that the biggest energy requirement occurs in first time period. This situation is clearly seen in Fig. 5. Also, the heat transfer rate increases as the shell radius and the length of TES decreases and the effect of length on the heat transfer rate decreases as shell radius increases.

Furthermore, the effect of operating parameters on the heat transfer rate for $R_{inf} = 3$ and $X_L = 100$ is illustrated in Fig. 6. The heat transfer rate increases as Reynolds number increases and inlet temperature of HTF decreases. But, the effect of inlet temperature is more significant than that of Reynolds number.

Fig. 7 shows the total thermal energy stored as a function of time for different operating parameters and $Re = 1000$ and $T_{in} = -15\,^{\circ}C$. The higher shell radius, the higher total charging time, dramatically. The case of $R_{in} = 5$ is not realistic since the total dimensionless charging time in this case is about 60, which corresponds to around 63 hours. The higher shell radius, the higher maximum total energy stored value since storing volume per TES unit increases with shell radius.

Fig. 8 presents the time-wise variation of total energy stored for different operating parameters. The shell radius and length

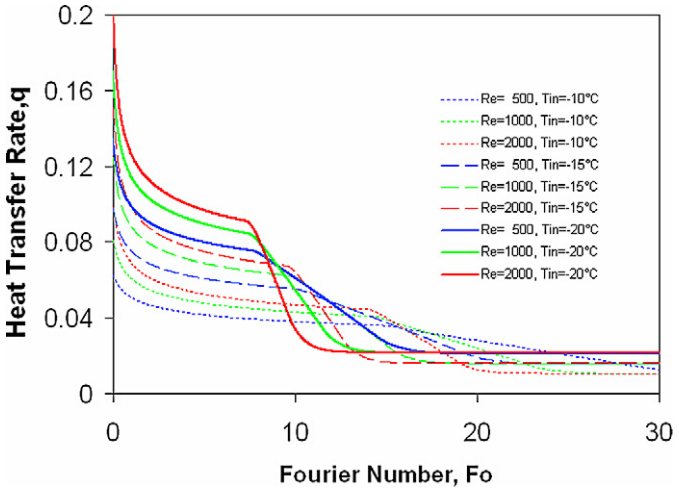

Fig. 6. Effect of operating parameters on heat transfer rate for $R_{\text{inf}} = 3$ and $X_L = 100$.

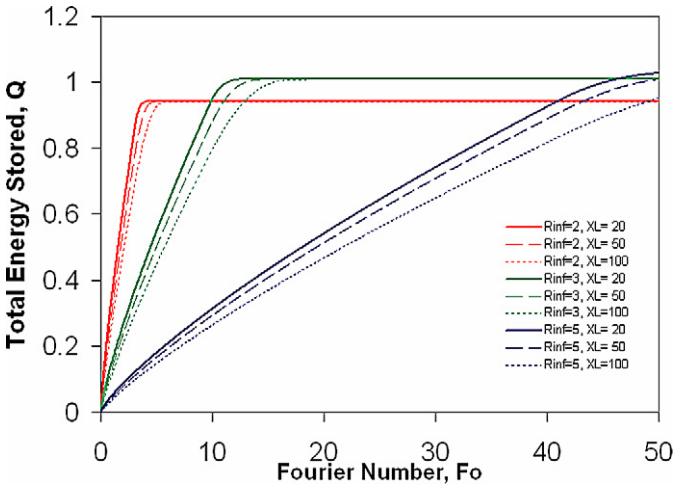

Fig. 7. Effect of design parameters on total energy stored for $Re = 1000$ and $T_{\text{in}} = -15\,^{\circ}\text{C}$.

are 3 and 100 in this figure, respectively. As explained in previous sections, the effect of inlet temperature on total energy storage is more significant than that of Reynolds number.

The entropy generation number, N_s, states total entropy generation in a system in dimensionless form. The entropy generation number in CTES system increases with time in charging process since the heat gain causes noteworthy amount of irreversibility. If the heat gain was not taken into account, the entropy generation number would be expected to decrease after solidification process almost finished. Fig. 9 shows the entropy generation number and exergy efficiency of whole system and the entropy generation number of HTF in order to show relation between entropy generation number and exergy efficiency. In this figure, Reynolds number, inlet temperature of HTF, the shell radius and length are taken as 1000, −15, 3 and 50, respectively. The entropy generation number and exergy efficiency of whole system are calculated from Eqs. (19) and (18), respectively. Note that the entropy generation in HTF is written as

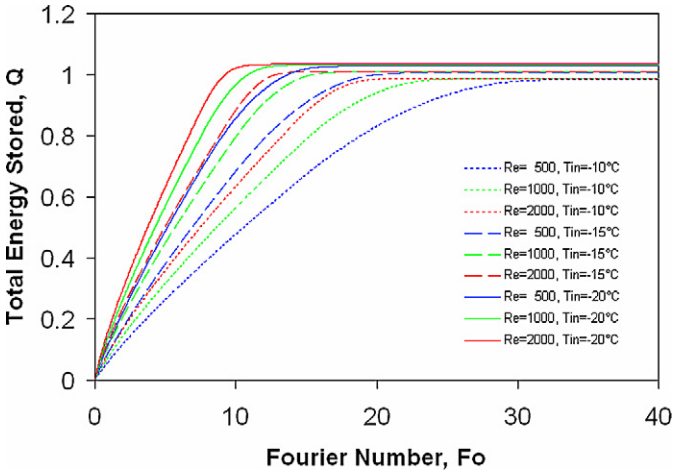

Fig. 8. Effect of operating parameters on total energy stored for $R_{\text{inf}} = 3$ and $X_L = 100$.

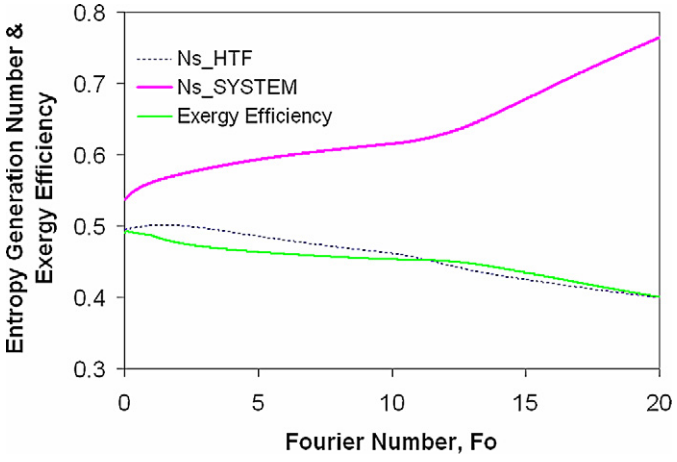

Fig. 9. Relation with entropy generation number and second law (exergy) efficiency.

$$S_{\text{gen,HTF}} = \int_{t=0}^{t} \left[\dot{m} c_{P,\text{HTF}} \ln\left(\frac{T_{\text{out}}(t)}{T_{\text{in}}} \right) - \frac{q^0(t)}{\bar{T}_{\text{PCM}}} + \Delta \dot{S}_{\text{HTF}} \right] \mathrm{d}t$$

Because of irreversibility due to the heat gain, the entropy generation number of system increases continuously with time whereas the exergy efficiency decreases with time. The gradient of curve increases after a certain time when thermal storage process finished since the temperature of system is almost inlet temperature of HTF and consequently, irreversibility occurring heat transfer from the environment is high at that time. However, the entropy generation number of HTF decreases after a certain time since the temperature difference between PCM and HTF decreases and the heat transfer from PCM to HTF occurs with reversible process.

Fig. 10 represents the effect of design parameters on the entropy generation number as a function of time for $Re = 1000$ and $T_{\text{in}} = -15\,^{\circ}\text{C}$. As shown in the figure, the entropy generation number has a small value in case of small value of shell radius in two time periods of the charging process. The higher the shell radius, the higher the entropy generation number in

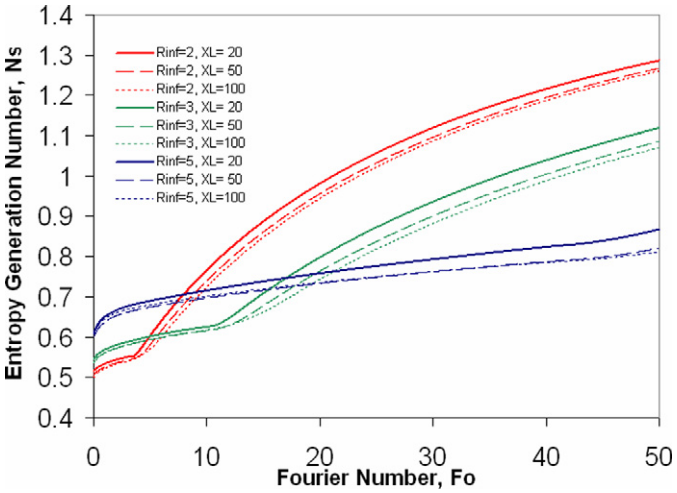

Fig. 10. Effect of design parameters on entropy generation number for $Re = 1000$ and $T_{in} = -15\,^{\circ}C$.

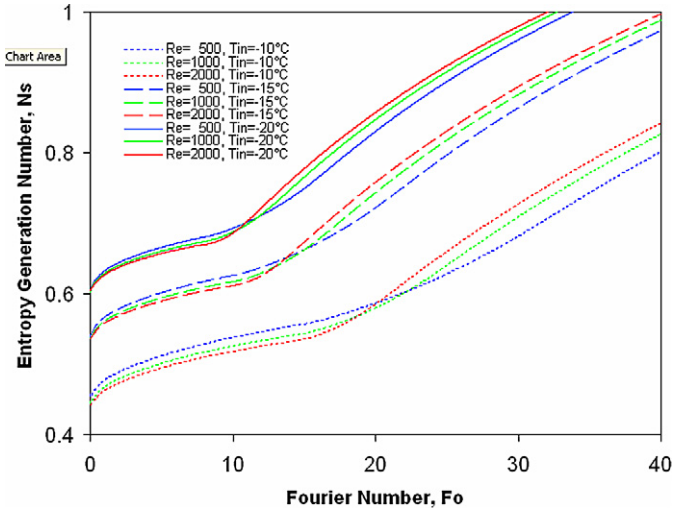

Fig. 11. Effect of operating parameters on entropy generation number for $R_{inf} = 3$ and $X_L = 100$.

that time periods. In contrast, the effect of length of TES on entropy generation number is not significant.

The variation of entropy generation number with Fourier number for different values of Reynolds number and inlet temperature where $R_{inf} = 3$ and $X_L = 100$ is shown in Fig. 11. The considerable influence of inlet temperature of HTF on entropy generation number is obvious from this figure. While at a fixed inlet temperature of HTF, as Reynolds number changes, the entropy generation number does not vary significantly.

Conclusions

In this paper we have undertaken a modeling study on entropy and exergy efficiency analysis during charging process of a cylindrical latent heat storage system. Some extensive parametric studies are also conducted to investigate how the solidification fronts, heat stored, heat transfer rates, entropy generation number and exergy efficiency change with time, particularly dimensionless time (the Fourier number). Also, the model results are then compared with some experimental data of one of the authors, and a good agreement is obtained for various parameters. The results show that entropy generation is crucial in such systems and should be minimized in order to increase the exergy efficiency and hence the system performance. Here are some specific results:

- Heat gain per volume increases as shell radius and length of the storage module decrease.
- Heat transfer rate increases as shell radius and length of the storage module decrease. The effect of length on the heat transfer rate decreases as the shell radius increases.
- Heat transfer rate increases with increasing *Re* number decreasing the inlet temperature of HTF. The temperature effect is more dominant than the *Re* number here.
- Entropy generation number increases with higher shell radius and is not significantly affected by the tube length and the *Re* number.

The results show that the most important design parameter is the shell radius and that optimum radius should be selected for better performance.

Acknowledgement

The authors acknowledge the support provided by Dokuz Eylul University in Turkey, and University of Ontario Institute of Technology and the Natural Sciences and Engineering Research Council in Canada.

References

[1] E.R.G. Eckert, R.J. Goldstein, W.E. Ibele, S.V. Patankar, Heat transfer a review of 1994 literature, Int. J. Heat Mass Transfer 40 (1997) 3729–3804.
[2] A. Saito, Recent advances in research on cold thermal energy storage, Int. J. Refrigeration 25 (2002) 177–189.
[3] I. Dincer, M.A. Rosen, Thermal Energy Storage Systems and Applications, John Wiley and Sons, London, 2002.
[4] B. Zalba, J.M. Marin, L.F. Cabeza, H. Mehling, Review on thermal energy storage with phase change: materials, heat transfer analysis and applications, Appl. Thermal Engrg. 23 (2002) 251–283.
[5] K.A.R. Ismail, C.L.F. Alves, Analysis of the shell-and-tube PCM storage system, in: Proceedings of the 8th International Heat Transfer Conference, 1986, pp. 1781–1786.
[6] Y. Cao, A. Faghri, Performance characteristics of a thermal energy storage module: a transient PCM/forced convection conjugate analysis, Int. J. Heat Mass Transfer 34 (1991) 93–101.
[7] Y. Cao, A. Faghri, A PCM/forced convection conjugate transient analysis of energy storage systems with annular and countercurrent flows, ASME J. Heat Transfer 113 (1991) 37–42.
[8] M. Lacroix, Study of the heat transfer behaviour of a latent heat thermal energy storage unit with a finned tube, Int. J. Heat Mass Transfer 36 (1993) 2083–2092.
[9] C. Bellecci, M. Conti, Phase change thermal storage: transient behaviour analysis of a solar receiver/storage module using the enthalpy method, Int. J. Heat Mass Transfer 36 (1993) 2157–2163.
[10] Y. Zhang, A. Faghri, Analytical solution of thermal energy storage system with conjugate laminar forced convection, Int. J. Heat Mass Transfer 39 (1996) 717–724.
[11] A.H.W. Lee, J.W. Jones, Modeling of an ice-on-coil thermal energy storage system, Energy Conversion and Management 37 (10) (1996) 1493–1507.

[12] A. Erek, Z. Ilken, M.A. Acar, Experimental and numerical investigation of thermal energy storage with a finned tube, Int. J. Energy Res. 29 (2005) 283–301.
[13] A. Erek, M.A. Ezan, Experimental and numerical study on charging processes of an ice-on-coil thermal energy storage system, Int. J. Energy Res. 31 (2007) 158–176.
[14] K. Ermis, A. Erek, I. Dincer, Heat transfer analysis of phase change process in a finned-tube thermal energy storage system using artificial neural network, Int. J. Heat Mass Transfer 50 (2007) 3163–3175.
[15] A. Trp, An experimental and numerical investigation of heat transfer during technical grade paraffin melting and solidification in a shell-and-tube latent thermal energy storage unit, Solar Energy 79 (2005) 648–660.
[16] A. Trp, K. Lenic, B. Frankovic, Analysis of the influence of operating conditions and geometric parameters on heat transfer in water–paraffin shell-and-tube latent thermal energy storage unit, Appl. Thermal Engrg. 26 (2006) 1830–1839.
[17] W.M. Kays, M.E. Crawford, Convective Heat and Mass Transfer, McGraw–Hill, New York, 1980.
[18] Y. Zhang, A. Faghri, Heat transfer enhancement in latent heat thermal energy storage system by using the internally finned tube, Int. J. Heat Mass Transfer 39 (1996) 3165–3173.
[19] S.V. Patankar, Numerical Heat Transfer and Fluid Flow, McGraw–Hill, New York, 1980.
[20] S.L. Lee, A strongly implicit solver for two-dimensional elliptic differential equations, Numer. Heat Transfer 16 (1989) 161–178.
[21] A. Bejan, Entropy Generation Minimization, CRC, New York, 1995.
[22] A. Bejan, I. Dincer, S. Lorente, A.H. Reis, A.F. Miguel, Porous Media in Modern Technologies: Energy, Electronics, Biomedical and Environmental Engineering, Springer-Verlag, New York, 2004.